IOP Publishing Semiconductor Science and Technology
Semicond. Sci. Technol. **29** (2014) 084003 (14pp) doi:10.1088/0268-1242/29/8/084003

Invited Article

Hexagonal boron nitride for deep ultraviolet photonic devices

H X Jiang and J Y Lin

Department of Electrical and Computer Engineering, Texas Tech University, Lubbock, TX 79409, USA

E-mail: hx.jiang@ttu.edu

Received 12 December 2013, revised 31 January 2014
Accepted for publication 7 February 2014
Published 6 June 2014

Abstract

This paper provides a brief overview on recent advances in tackling the doping and optical polarization issues involved in the development of high performance deep ultraviolet (DUV) light emitting devices. In particular, recent developments in the exploitation of a novel DUV emitter layer structure based on a hexagonal boron nitride (hBN) and AlGaN p–n junction and doping engineering to potentially overcome the intrinsic problem of low p-type conductivity (or low free hole concentration) in Al-rich AlGaN are summarized. By implementing the wide bandgap and highly conductive hBN p-type layer strategy in nitride DUV emitters, p-type conductivities and DUV transparency of the electron blocking layer and p-type contact layer will be dramatically increased. This will significantly improve the free hole injection and quantum efficiency, reduce the operating voltage and heat generation, and increase the device operating lifetime. The growth of undoped and Mg-doped p-type hBN via a metal organic chemical vapor deposition technique has been studied. Furthermore, p-hBN/n-AlGaN p–n junctions have been fabricated and characterized to demonstrate the feasibility and potential of p-hBN/n-AlGaN p–n heterostructure based DUV light emitting devices. Further improvements in material quality, p-type conductivity control and device processing procedures would enhance the properties of these p–n structures, which could *ultimately pave the way* towards the realization of high efficiency nitride DUV photonic devices.

Keywords: ultraviolet, photonic, hexagonal, boron nitride, devices

(Some figures may appear in colour only in the online journal)

Introduction

There is a great need for the development of chip-scale deep ultraviolet (DUV) light sources for a wide range of applications in areas of probing intrinsic fluorescence in a protein, medical equipment/personnel decontamination and sterilization and photocatalysis [1, 2]. The applications of present DUV systems are limited by cost, size, weight, power requirement and performance capability. The realization of chip-scale DUV light sources would provide significant benefits in terms of cost and volume, as well as allow for integration with other functional devices. However, realizing DUV emitters with high external quantum efficiency (EQE) is extremely challenging. Among all semiconductors, III-nitride materials (AlInGaN material system), Al-rich AlGaN ternary alloys in particular, have been the default choice for the development of efficient light emitting diodes (LEDs) and laser diodes (LDs) operating at wavelengths below 300 nm. As a whole, the nitride community has overcome, to a certain extent, several key issues facing DUV materials and devices. Various groups in the world have obtained DUV LEDs [3–17]. The EQE among the best DUV LEDs is around 10% or below for devices operating around 270–280 nm at 20 mA [14, 15]. The EQE of LEDs operating in the UV-C spectral region (around 250 nm) is still quite low (below 3%) [16, 17]. Many technological challenges remain to be overcome for the realization of high performance LEDs operating in the UV-C range, which is the most effective wavelength for the destruction of the nucleic acids in micro-organisms such as pathogens and viruses.

A typical DUV emitter layer structure employing AlGaN is shown in figure 1. In general, DUV emitter material structure is optimized based on the studies of Al-rich *n*- and

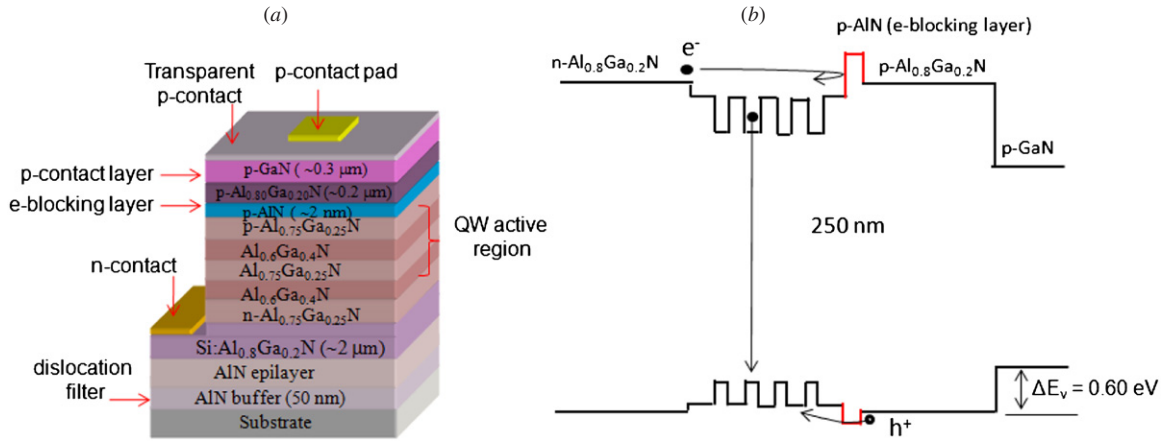

Figure 1. Schematic diagram of the conventional DUV device approach: (*a*) schematic layer structure and (*b*) the corresponding energy band diagram of the device layer structure. The e-blocking layer based on AlN or Al-rich AlGaN is generally highly resistive due to the large activation energies of Mg acceptors in AlN and Al-rich AlGaN, which cause very low hole injection efficiencies. The use of a p-GaN contact layer also reduces the DUV transparency.

p-AlGaN. A high-temperature AlN epitaxial layer (epi-template) is grown on a substrate (e.g., sapphire). This is then followed by the growth of an undoped Al-rich AlGaN layer and a highly conductive Si-doped Al-rich *n*-AlGaN cladding layer, followed by a quantum well (QW) active region consisting of alternating layers of AlGaN wells/AlGaN barriers and then a Mg-doped AlGaN electron blocking layer. Since it is difficult to achieve a reasonable hole concentration in an AlGaN alloy with high Al composition, a Mg-doped high Al-content AlGaN layer is generally employed as an electron blocking (e-blocking) layer to block the electron overflow into the p-type layers, thereby enhancing the electron–hole radiative recombination in the QWs. The structure is then completed with a *p*-AlGaN cladding layer, and a highly doped p-GaN thin contact layer. Al mole fraction can be adjusted depending on the target emission wavelength. In general, the barrier layers in the QW active region have similar Al mole fractions as the n- and p-type cladding layers, while the well region has the lowest Al mole fraction (except for the p-GaN contact layer) and the electron blocking layer has the highest Al mole fraction and thus is the most resistive layer in the entire structure.

Inspecting the DUV emitter layer structure shown in figure 1, several significant challenges can be identified. These include issues of *achieving* a highly conductive *n-type* Al-rich AlGaN cladding layer for electron injection and light extraction from the inherently edge-emitting [18] Al-rich AlGaN. However, the most outstanding issue is the low conductivity of p-type AlGaN, which is intrinsic to AlGaN. This issue is caused by the large acceptor activation energies (E_A) in $Al_xGa_{1-x}N$ (as large as 500–600 meV in AlN) [8, 19–23]. As shown schematically in figure 1, III-nitride DUV emitters must incorporate an e-blocking layer with a larger band gap than the active region to maximize the electron–hole radiative recombination in the QW active region. The AlGaN e-blocking layer is the most resistive p-layer in the device structure. Unfortunately, this highly resistive e-blocking layer must have a certain thickness in order to stop the electrons overflow into the p-layers and to eliminate the unwanted long wavelength emission caused by the recombination between electrons and Mg impurities in the p-type layers. Thus, the highly resistive nature of this e-blocking layer is one of the primary causes of low hole injection efficiency and, consequently, the low QE of nitride DUV emitters. Although various interesting methods and schemes, such as enhancing p-type doping via minimizing the densities of hole compensating centers such as nitrogen vacancies with three (V_N^{3+}) or one (V_N^{1+}) positive charges [22–26], polarization and piezoelectric doping [27], p-AlGaN graded layers [28, 29], p-multiple quantum wells or superlattices [11, 30, 31], etc have been implemented to overcome the problem of low hole injection efficiency to a certain degree, significant advances in the EQE of DUV emitters will require the exploitation of disruptive device concepts.

In this paper, we first briefly discuss earlier works on achieving highly conductive n-type AlGaN with high Al-contents and techniques to enhance the light extraction from the inherently edge emitting AlN and Al-rich AlGaN due to their fundamental band structures. The focus of this paper is to provide a brief summary on the recent developments on the exploitation of a novel DUV emitter layer structure based on hexagonal boron nitride (hBN) and AlGaN p–n junction engineering to potentially overcome the most daunting p-type doping challenge facing the development of high performance DUV light emitting devices based on Al-rich AlGaN alloys.

Achieving highly conductive n-type Al-rich AlGaN

Achieving highly conductive n-type $Al_xGa_{1-x}N$ alloys with high Al contents was considered to be challenging due to: (i) an increase in the ionization energy of the Si donors with increasing Al content, from around 20 meV in GaN to about 180 meV in AlN [32] and (ii) the formation energy of cation vacancy (V_{III}) decreases with increasing Al content and becomes very low with a triple negatively charged state in AlN, $(V_{III})^{3-}$ [25, 26, 33, 34]. Prior to 2002, only insulating Al-rich $Al_xGa_{1-x}N$ ($x > 0.5$) can be obtained. Considering the fact that the donor activation energy in AlN is comparable to

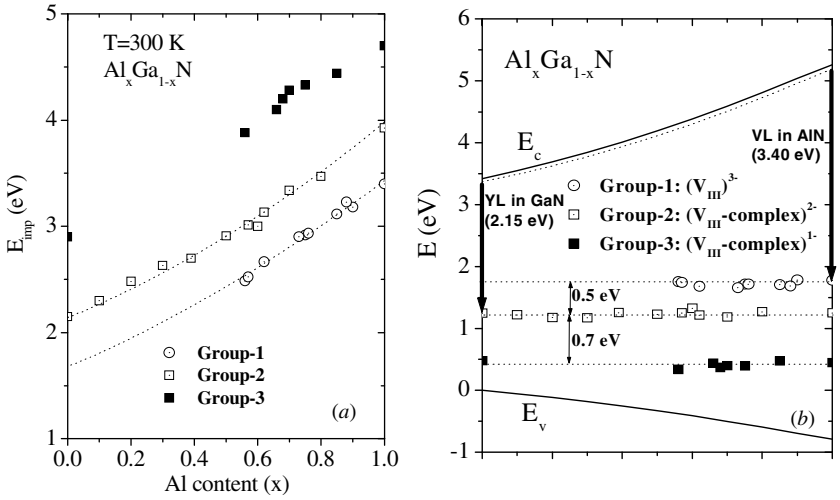

Figure 2. (*a*) PL peak position of the impurity transitions of the three groups in $Al_xGa_{1-x}N$ as functions of Al content x. Dotted lines are guide to the eyes [After Ref. 9]. (*b*) The deep acceptor energy levels associated with $(V_{III})^{3-}$, $(V_{III}\text{-complex})^{2-}$ and $(V_{III}\text{-complex})^{1-}$, plotted as a function of the Al content, x [after Refs. 35, 36].

the Mg acceptor ionization energy in GaN, it is more important to minimize the density of cation-vacancy-related-deep-level impurities which act as the free electron compensating centers (or electron traps) for n-type doping, in order to increase the conductivities of *n*-$Al_xGa_{1-x}N$ with high Al-contents. Consequently, finding effective methods for the identification of cation vacancies in AlGaN is very important for designing growth experiments to eliminate these defects.

By employing the DUV photoluminescence (PL) spectroscopy, we have identified three groups of deep impurity transitions in Si-doped $Al_xGa_{1-x}N$ [35–39]. In figure 2, we plot the room temperature PL spectral peak position (E_{imp}) of these three groups of impurity transitions in $Al_xGa_{1-x}N$ alloys as functions of x. The physical origins of these three groups of transition lines were ascribed to the deep level acceptors with triple, double and single negatively charged states.

Group-1. A donor–acceptor-pair (DAP) transition involves a shallow donor and an isolated Al vacancy deep acceptor with triple negatively charged state $(V_{Al})^{3-}$ in $Al_xGa_{1-x}N$ alloys between $x \approx 0.58$ and 1. The group-1 transitions include the commonly observed violet line (VL) appearing at about 3.40 eV in AlN. The presence of $(V_{Al})^{3-}$ is most detrimental to n-type doping because each defect can trap three free electrons.

Group-2. A DAP transition between a shallow donor level to a deep acceptor level involving cation vacancy complex with double negatively charged state $(V_{III}\text{-complex})^{2-}$ such as V_{III}–O_N or V_{III}–Si_{III} in $Al_xGa_{1-x}N$ alloys between $x = 0$ and 1. The group-2 transitions include the well-known yellow line (YL) appearing at about 2.15 eV in GaN ($x = 0$). The presence of $(V_{III}\text{-complex})^{2-}$ is also detrimental to n-type doping because each defect can trap two free electrons.

Group-3. A DAP transition involves a shallow donor and a deep acceptor level involving cation vacancy complex with single negatively charged state $(V_{III}\text{-complex})^{1-}$ deep acceptor such as $(V_{Al}\text{-}2O_N)^{1-}$ in $Al_xGa_{1-x}N$ alloys between $x = 0$ and 1. AlGaN alloys predominantly exhibiting the band edge and the group-3 transitions possess improved conductivities over those emitting predominantly group-2 and group-3 transitions.

It is interesting to note that the energy levels of these three deep acceptors in $Al_xGa_{1-x}N$ alloys increase with x and are pinned to common energy levels in vacuum, as illustrated in figure 2(*b*). The calculated binding energy of $(V_{Al}\text{-}2O_N)^{1-}$ ranges from 1.0 to 1.12 eV in AlN [33, 34]. The calculated differences in binding energies between $(V_{III})^{3-}$ and $(V_{Al}\text{-}O_N)^{2-}$ and between $(V_{Al}\text{-}O_N)^{2-}$ and $(V_{Al}\text{-}2O_N)^{1-}$ in AlN, respectively, are about 0.5 and 0.7 eV [33, 34], which agree quite well with the experimentally measured values shown in figure 2. The presence of dislocations can enhance the formation of cation vacancies during the nitride crystal growth. Thus, a high dislocation density generally translates to a reduced conductivity in AlGaN and AlN. One effective way to reduce the densities of cation-vacancy-related-deep-level impurities is by inserting a high-quality AlN epilayer that serves as a template/dislocation filter for the subsequent growth of AlGaN alloys. Over the past decade, many groups in the world have established the benefits of inserting an AlN epilayer as a template for the growth of subsequent III-nitride DUV device structures on sapphire and the approach has become a standard today [4–17, 40–42]. Compared to GaN, dislocations are more difficult to propagate through the AlN template due to its stronger bonds. For *c*-plane AlN epilayers, a previous work has also indicated that screw type dislocations mostly stopped propagating along the (0 0 0 2) direction within a thickness of 0.5 μm [43]. By monitoring and minimizing the deep level impurity transition lines while varying the growth conditions and layer structures, highly conductive Al-rich AlGaN alloys have been routinely obtained. As of today, n-type conductivity control in Al-rich AlGaN is no longer considered an issue for DUV emitter implementation. For instance, Hall measurement results shown in figure 3(*a*) indicate that n-type Al-rich $Al_xGa_{1-x}N$ ($x > 0.7$) epilayers with very high electrical conductivities have been achieved ($\rho = 0.0075$ Ωcm, $n = 3.3 \times 10^{19}$ cm^{-3} $\mu = 25$ cm^2 Vs^{-1} at 300 K for $Al_{0.7}Ga_{0.3}N$) [32, 44]. The Si donor activation energy in $Al_xGa_{1-x}N$ ($x >$

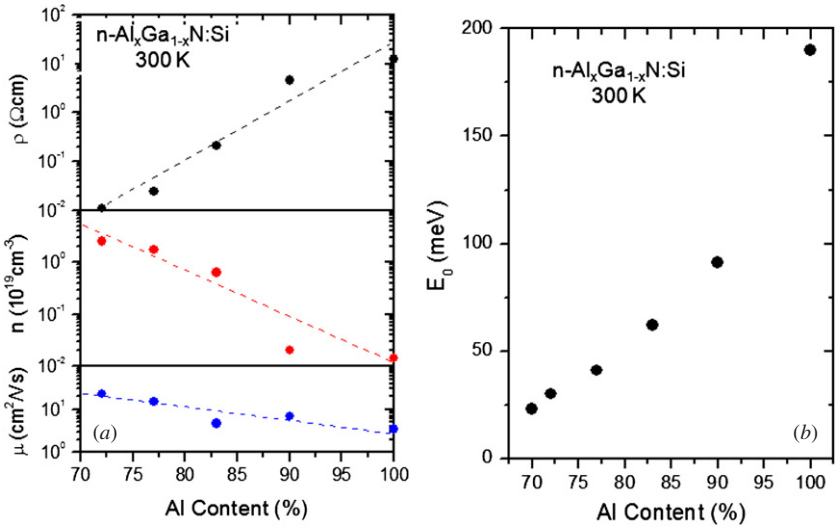

Figure 3. (*a*) Room temperature Hall measurement results including resistivity, electron concentration, and electron mobility of Si-doped n-$Al_xGa_{1-x}N$ ($x > 0.7$) epilayers grown on AlN-epilayer/sapphire templates. Results indicate that n-type Al-rich $Al_xGa_{1x}N$ ($x > 0.7$) epilayers with very high conductivities have been achieved (for example, for $Al_{0.7}Ga_{0.3}N$, $\rho = 0.0075$ Ωcm, $n = 3.3 \times 10^{19}$ cm^{-3} $\mu =$ 25 cm^2 Vs^{-1} at 300 K); (*b*) Si donor activation energy in $Al_xGa_{1-x}N$ ($x > 0.7$) epilayers as a function of the Al content, x, estimated from the temperature-dependent resistivity results [after Refs. 32, 44].

0.7) epilayers as a function of the Al content, x, estimated from the temperature-dependent resistivity results is also shown in figure 3(*b*).

Optical polarization in *c*-plane Al-rich AlGaN alloys and QWs and light extraction

AlN is the only wurtzite (WZ) semiconductor compound that has been predicted to have a negative crystal field splitting in the valence bands [45–48]. The band structures and properties of the fundamental optical transitions near the band edges of AlN and GaN have been studied [18, 49–51]. As shown in figure 4(*a*), the conduction bands have a Γ_7 symmetry in both AlN and GaN. Compared with the band structure of GaN, the most significant difference in AlN is the negative crystal-field splitting Δ_{CF} (−213 meV) compared with a positive value (+38 meV) in GaN [49–51]. Because of this large negative Δ_{CF} in AlN, the order of the valence bands in AlN is different from that in GaN. The top valence band has Γ_7 (Γ_9) symmetry in AlN (GaN) because of the negative (positive) Δ_{CF}. Therefore, light emission due to the recombination between the conduction band electrons and the holes in the top valence band is polarized with E//c in AlN, which is in contrast to that in GaN (E⊥c). The unique band structure of AlN affects profoundly the optical properties of Al-rich AlGaN alloys. One distinctive example is presented in figure 4(*b*), which shows that with increasing x, the dominant emission component in $Al_xGa_{1-x}N$ evolves from transverse electric (TE) polarization (E⊥c) in GaN to transverse magnetic (TM) polarization (E//c) in AlN [18]. This is a direct consequence of the band structure—the valence band with Γ_7 symmetry evolves from the lowest valence band in GaN to the topmost valence band in AlN. Our polarization resolved PL measurement results shown in figures 4(*b*) and (*c*) suggest that this transition occurs at $x \approx$ 0.25 in $Al_xGa_{1-x}N$ epilayers [18].

The polarization of light emission from AlGaN has a profound influence on the UV LED external efficiency [18, 52]. As illustrated in figure 5, the light extraction in a QW LED in general is limited to a small cone, defined by the refractive index contrast between the semiconductor material and the environment (air or encapsulation). Typically, this cone is smaller than ∼20°. Only the photons emitted in this cone (propagating toward the outlet of the cone) can be extracted, while others form a guided wave in the cladding layer, and finally are absorbed by the semiconductor defects. For most semiconductor materials covering infrared to blue wavelength, the polarization of the emitted light is mainly (**E**⊥**c**) and parallel to the surface plane [53], i.e. the propagation of the light is toward the surface, so the emitted photons in the cone can be extracted. Unfortunately, for AlGaN-based DUV LEDs, the emitted light has a polarization of (**E**//**c**) and perpendicular to the surface plane, i.e. emitted light propagates laterally within the semiconductor layer. In other words, Al-rich AlGaN alloys and QWs are inherently edge-emitting materials and DUV devices based on these materials tend to have TM polarization.

To enhance the transverse light extraction in DUV LEDs, introducing deep surface features into the cladding and QW layers will allow the TM polarized light to be extracted from the surface. Of the different schemes, photonic crystals (PC) [54–57] and micro-LED (μLED) arrays [58–64] are very promising approaches. Figures 6 and 7 show examples of PC-LEDs and μLED arrays to enhance the light extraction efficiency. A 20-fold enhancement of light extraction using optical pumping was demonstrated. For UV PC-LEDs under current injection [54], a three-fold enhancement in light extraction [55, 56] and a four-fold enhancement in modulation speed [57] have been realized by PC formation. In addition to the ability for enhancing the light extraction, when individually addressed the III-nitride μLED arrays form solid-state self-emissive microdisplays with outstanding attributes include

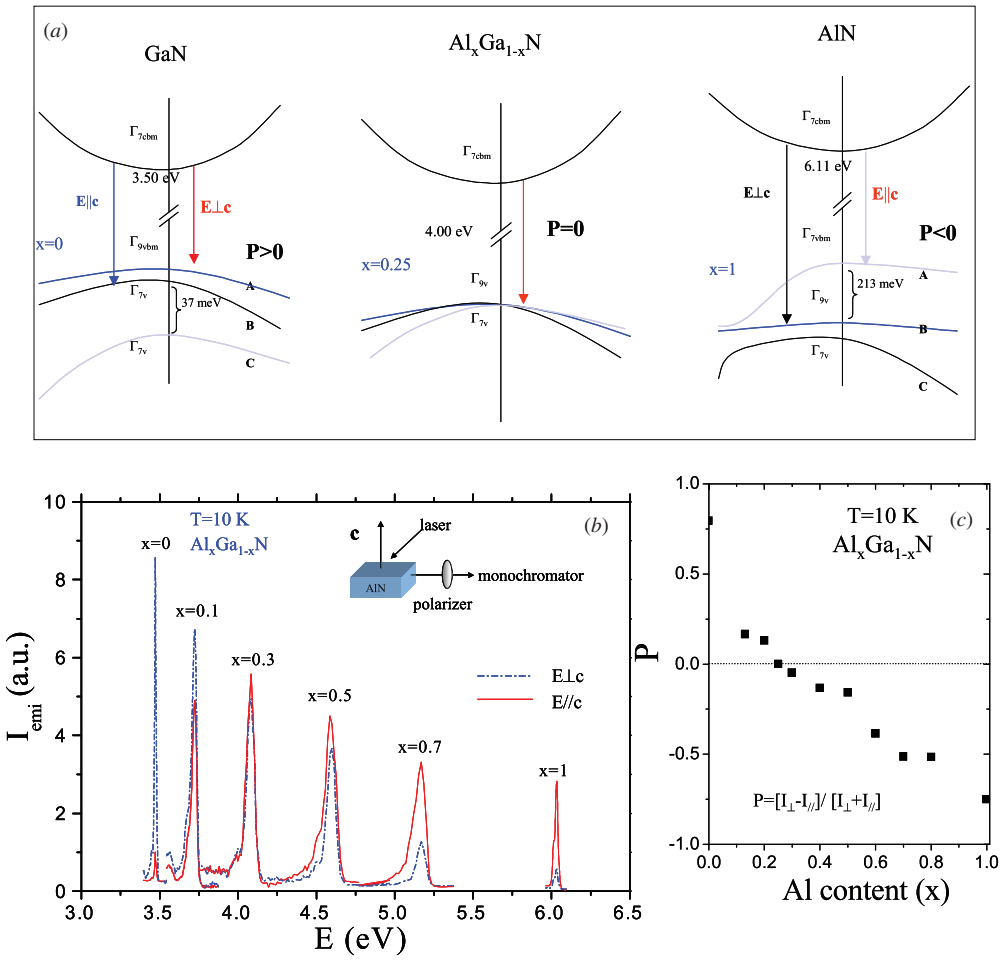

Figure 4. *(a) The band structures near the* Γ*-point of* $Al_xGa_{1-x}N$ alloys for GaN ($x = 0$) [after Ref. 49], $Al_xGa_{1-x}N$ ($x = 0.25$) [after Ref. 18], and AlN ($x = 1$) [after Ref. 50]. (*b*) Low temperature (10 K) PL spectra of $Al_xGa_{1-x}N$ alloys of varying x, from $x = 0$ to 1 [after Ref. 18]. The experimental geometry was depicted in the inset, where the electrical field of PL emission (**E**) can be selected either parallel (//) or perpendicular (⊥) to the **c** axis of the crystal. The dominant emission component in $Al_xGa_{1-x}N$ evolves from **E**⊥**c** (in GaN) to **E**//**c** (in AlN) [18]. (*c*) The degree of polarization P versus x in $Al_xGa_{1-x}N$ alloys [after Ref. 18].

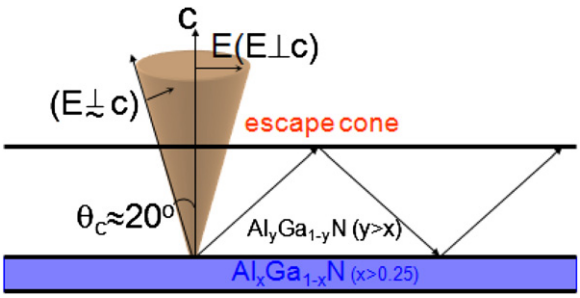

Figure 5. Schematic diagrams of light extraction cone of UV LEDs based on $Al_xGa_{1-x}N$.

high brightness, efficiency and robustness [65–68]. When serially connected on chip, III-nitride μLED arrays form high voltage single-chip AC/DC-LEDs without power converters to address the key compatibility issue between LEDs and ac power grid infrastructure [68–71].

For laser diode (LD) applications, although the edge emission property of Al-rich $Al_xGa_{1-x}N$ is considered to be not a problem, TE polarized LDs are generally preferred for practical implementation. By carefully designing the QW structures with reduced QW width, the quantum confinement can be utilized to alter the valence-band order and, consequently promotes TE (**E**⊥**c**) polarization in Al-rich $Al_xGa_{1-x}N$ QWs [72–74]. As a result, the transition from **E**⊥**c** to **E**//**c** may occur at much larger x values. For instance, for AlN/$Al_xGa_{1-x}N$ QWs ($x \approx 0.65$) the predominant polarization switches from **E**//**c** to **E**⊥**c** if the well width is engineered to be 2 nm or below [74].

p-type doping challenge

Among the many technological challenges for the realization of high performance DUV emitters, the most outstanding issue is the low conductivity of p-type AlGaN. This issue is fundamental to AlGaN and is caused by the large acceptor activation energies (E_A) of $Al_xGa_{1-x}N$ (as large as 500 meV in AlN) [8, 19–23]. The detrimental effects of the large acceptor activation energies in Al-rich AlGaN on the QE of DUV emitters can be further understood by the following reasons. As shown in figure 8(*a*), the Mg acceptor level in $Al_xGa_{1-x}N$ increases with increasing x, from about 170 meV ($x = 0$) to 530 meV ($x = 1$). The resistivity (ρ) increases exponentially

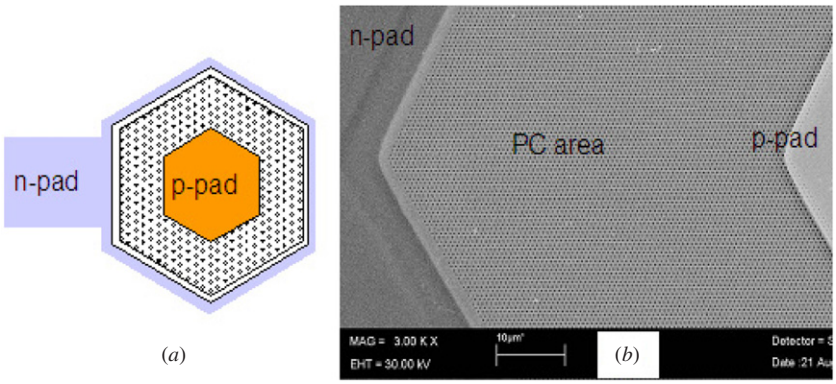

Figure 6. (*a*) Schematic of photonic crystal (PC) incorporation on III-nitride emitters and (*b*) scanning electron microscopy (SEM) image of PCs created by nanofabrication [after Refs. 56].

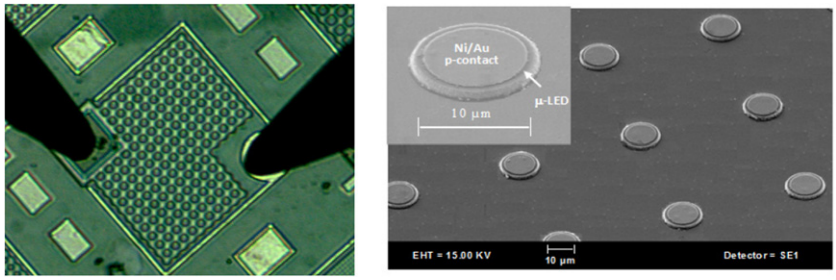

Figure 7. (*a*) An example of an interconnected μ-LED for boosting LED extraction efficiency; (*b*) SEM image of InGaN/GaN quantum well micro-size LED (μLED) array [after Refs. 58, also on the cover page of *Compound Semiconductor*, November 2000 issue].

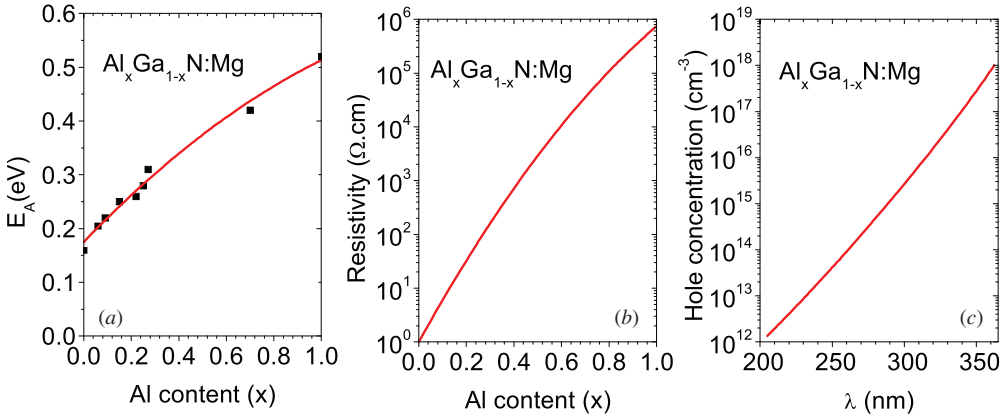

Figure 8. (*a*) The activation energy, E_A, of Mg acceptor in $Al_xGa_{1-x}N$ as a function of Al-content. (*b*) P-type resistivity of $Al_xGa_{1-x}N$, ρ_{AlGaN}, as a function of Al-content according to equation (1). In the plot, the typical p-type resistivity value of GaN, $\rho(GaN) = 1\ \Omega \cdot cm$ and E_A values from figure 8(*a*) are used. (*c*) Free hole concentration as a function of the emission wavelength of $Al_xGa_{1-x}N$ DUV LEDs. In the plot, $E_g = xE_g(AlN)+(1–x)E_g(GaN)+bx(1–x)$, $E_g(AlN) = 6.05$ eV, $E_g(GaN) = 3.42$ eV, $b = 0.98$ eV and the typical free hole concentration of Mg-doped GaN, $p_{GaN} = 1 \times 10^{18}\ cm^{-3}$ are used [after Refs. 8, 19–21].

with Al concentration (x) in Mg-doped $Al_xGa_{1-x}N$ alloys according to the following equation [8]:

$$\rho AlGaN = \rho GaN\ \exp(\Delta E_A/kT) = \rho GaN\ \exp\{[E_A(AlGaN) - E_A(GaN))]/kT\}, \quad (1)$$

where E_A is the activation energy of acceptors. Equation (1) is plotted in figure 8(*b*). For instance, for an optimized Mg-doped $Al_{0.7}Ga_{0.3}N$ epilayer, we have obtained a resistivity around $10^5\ \Omega \cdot cm$ at room temperature and confirmed p-type conduction only at elevated temperatures (>700 K) with a resistivity of about 40 $\Omega \cdot cm$ at 800 K [8]. Similarly, for Mg-doped AlN, p-type resistivity can only be probed at temperatures above 600 K [21]. On the other hand, the number of free holes (P) injected into the active region follows:

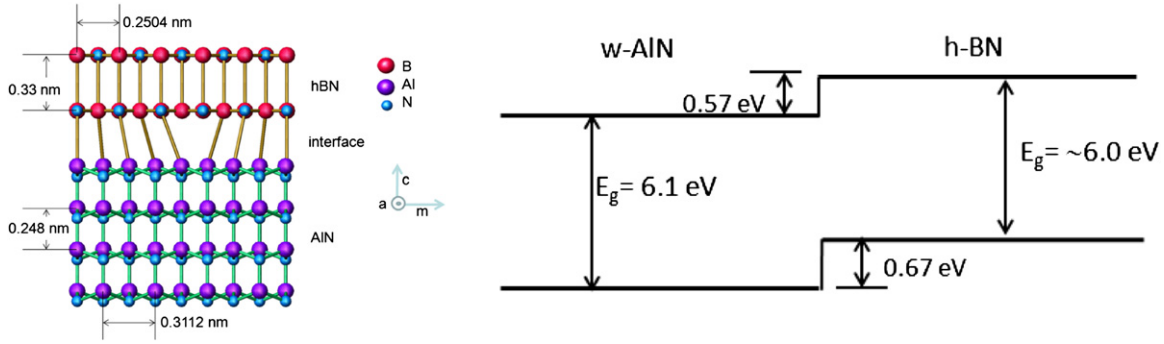

Figure 9. (*a*) Illustration of the heteroepitaxial growth of hexagonal boron nitride (hBN) on wurtzite AlN (w-AlN). Note that four *a*-lattice constants of AlN ($4\ a_{AlN} = 4 \times 0.3112$ nm $= 1.245$ nm) are almost the same as that of five *a*-lattice constants of hBN ($5\ a_{BN} = 5 \times 0.2504$ nm $= 1.252$ nm). This means that every five hBN atoms will align with four AlN along the *a*-direction. This 5/4 coincidence in the hBN/w-AlN heterojunction interface effectively reduces the lattice mismatch from 19.54% to about 0.58%. (*b*) Band edge alignment between hBN and w-AlN [after Refs. 80, 87].

$$P_{AlGaN} = P_{GaN}\exp(-\Delta E_A/kT) = P_{GaN}\exp\{-[E_A(AlGaN) - E_A(GaN))]/kT\}. \quad (2)$$

Equation (2) implies that the hole injection efficiency, or the QE of DUV LEDs, decreases exponentially with increasing Al-content or with decreasing the emission wavelength, as illustrated in figure 8(*c*). Since the free hole concentration (*P*) depends exponentially on the acceptor energy level, $P \sim \exp(-E_A/kT)$, an E_A value around 500 meV translates to only one free hole for roughly every two billion (2×10^9) incorporated Mg impurities (at 300 K). This causes an extremely low free hole injection efficiency into the QW active region. This is equivalent to saying that the QE of DUV LEDs decreases exponentially with decreasing the emission wavelength or increasing the emission energy, a fact that has been extensively observed and surveyed [1, 75].

We have also studied alternative p-type dopants in AlGaN. For instance, we have determined that the acceptor energy level of Zn (~0.6 eV) in AlN is even deeper than that of Mg in AlN [76]. We have come to the realization that the deepening of the acceptor level in $Al_xGa_{1-x}N$ with increasing *x* is a fundamental physics problem and that it is necessary to explore DUV device structures that exploit new p-type layer strategies in order to significantly improve the free hole injection efficiency in AlGaN DUV emitters.

Criteria for the choice of alternative p-type materials

The material of choice for new p-type layers in nitride DUV emitters must satisfy the following criteria.

(1) Structure and materials system must be compatible with AlGaN and AlN growth (so that single epi-growth is possible).
(2) Favorable band-edge alignment with AlGaN and AlN (to assist e-blocking and hole injection).
(3) Lower acceptor energy level than those in Al-rich AlGaN and AlN.
(4) Higher free hole concentrations than those in Al-rich AlGaN and AlN.

It turns out that hexagonal hBN satisfies all of the above criteria. Since p-type conductivity is such an overwhelming issue for improving the performance of nitride DUV emitters, we will describe each criterion below.

Criterion 1. The lattice mismatch is about 19.54% when the hBN epilayer is grown on a c-plane AlN epilayer. However, we noticed that four *a*-lattice constants of AlN ($4\ a_{AlN} = 4 \times 0.3112$ nm $= 1.245$ nm) is almost the same as five *a*-lattice constants of hBN ($5\ a_{BN} = 5 \times 0.2504$ nm $= 1.252$ nm), which means that every five hBN atoms will align with four AlN along the *a*-direction as illustrated in figure 9(*a*). This 5/4 coincidence in the hBN/w-AlN heterojunction interface reduces the effective lattice mismatch from 19.54% to about 0.58%. The feasibilities of depositing high-quality hBN epilayers on top of AlGaN [77] and AlGaN on hBN [78, 79] have been demonstrated via state-of-the-art epitaxial growth techniques such as metal organic chemical vapor deposition (MOCVD).

Criterion 2. Hexagonal BN provides the exact properties that are needed for nitride DUV LED p-layers (e-blocking and p-contact layers). Figure 9(*b*) shows the calculated band edge alignment between hBN and wurzite AlN (w-AlN) [80]. The calculation results showed that the band edge of hBN moved upwards with respect to that of w-AlN (type II alignment). This unique bandgap alignment between hBN and w-AlN will greatly aid the development of nitride DUV emitters in the following two important aspects:

- it helps electron blocking;
- it increases hole injection into the AlGaN QW active region.

This will help to solve the most critical issues in next generation nitride DUV emitters by providing sufficient free hole injection into the QWs while minimizing unwanted long wavelength emissions.

Criterion 3. Both calculation and previously reported results showed strong evidence that the acceptor activation energy in hBN is much smaller than that in AlN. The band structure calculation clearly shows a smaller effective hole mass in hBN ($m^* \approx 0.5\ m_o$) [81, 82] than in AlN (shown in

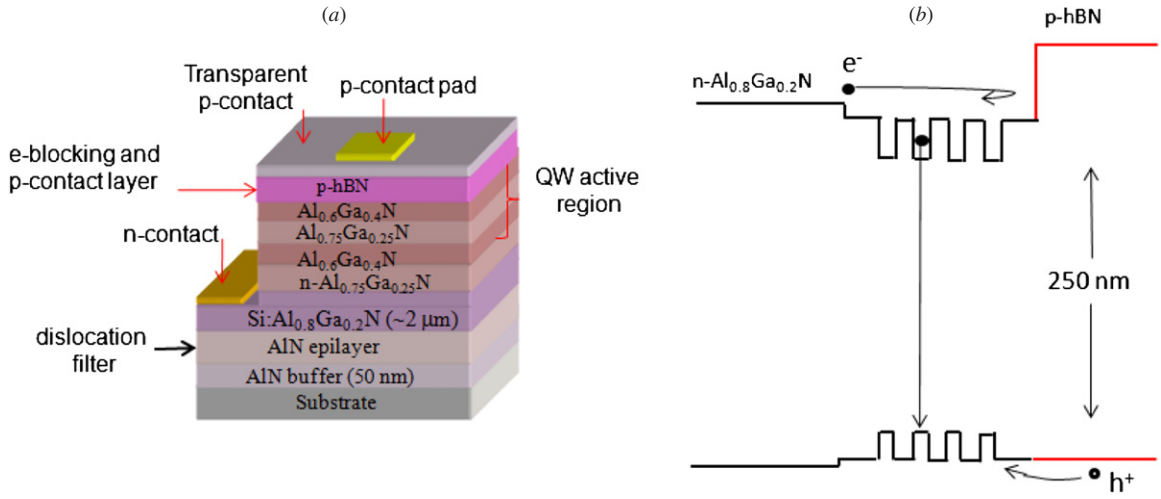

Figure 10. (*a*) Schematic of a novel DUV LED layer structure using p-type hexagonal boron nitride (hBN). The wide bandgap (~6 eV) p-hBN serves as a natural electron (e)-blocking and p-type contact layer and dramatically improves the hole injection efficiency in DUV LEDs. Our approach is based on hBN's unique band-edge alignment with AlGaN, excellent p-type conductivity and transparency to DUV photons. (*b*) The corresponding energy band diagram of our novel DUV LED layer structure [after Ref. 87].

Table 1. Comparison of basic parameters between hBN and w-AlN.

Crystal structure	Hexagonal BN	Wurtzite AlN
c-lattice constant (Å)	6.66	4.98
a-lattice constant (Å)	2.504	3.112
Energy gap (eV)	~6.0	6.1
Theoretical hole effective mass (m_0) in-plane, out-of-plane	0.5 (M→Γ) 1.33 (M→L)	3.53
Theoretical electron effective mass (m_0) in-plane, out-of-plane	0.26 (M→Γ) 2.21 (M→L)	0.3
Electronic bonding	SP^2	SP^3
Dielectric constant (in-plane)	4	8.5
Acceptor energy level, E_A (eV) (effective mass theory)	0.18	0.66
E_A (eV, measured)	0.03–0.3 (Mg)	~0.51 (Mg)
Measured hole concentration @ RT (cm^{-3})	1.5×10^{18}–2.7×10^{19}	$\sim 10^{12}$
Hole mobility ($cm^2/V \cdot s$)	2–26 (measured)	<5 (estimated)
p-type resistivity @ RT ($\Omega \cdot cm$) estimated (measured)	0.01 (2–10)	$> 10^6$

table 1), which indicates a lower E_A according to effective mass theory:

$$E_A = 13.6\ \text{eV}(m*/m^0)(\varepsilon_0/\varepsilon)^2, \quad (3)$$

where m^*, m^0, ε_0, ε are the effective hole mass in the semiconductor, effective hole mass in free space, dielectric constant in free space and dielectric constant in the semiconductor, respectively. The measured acceptor energy levels were 0.3 and 0.15 eV for Mg- and Zn-doped BN films of mixed phases prepared by CVD, sputtering and ion implantation [83–85]. The Mg acceptor level measured in epitaxial films of pure hexagonal phase with a relatively heavy doping prepared by MOCVD by our group is around 30 meV [86].

Criterion 4. Although lower E_A indicates higher free hole concentration, self-compensation could potentially reduce free hole concentration. Our preliminary results also indicated that self-compensation is less of a problem in hBN than w-AlN. This is possibly due to the smaller *a*-lattice contact of hBN compared to w-AlN. This will allow the attainment of higher p-type conductivity. In our preliminary studies, we have obtained Mg-doped hBN (hBN:Mg) with p-type resistivities ranging from 2 to 10 $\Omega \cdot$ cm and hole concentration P ~ 1 × 10^{18} cm^{-3} at room temperature [77, 86]. Much more works are needed to further improve the overall material quality and hence hole mobility and understanding the mechanisms of compensation defect generation and elimination. Nevertheless, the dramatic reduction in acceptor energy level and p-type resistivity by about 5 to 6 orders of magnitude in hBN:Mg over AlN:Mg represents an exceptional opportunity to revolutionize the p-layer approach and overcome the intrinsic problem of p-type doping in Al-rich AlGaN, thus potentially solves one of the most difficult issues in III-nitride DUV emitters and opens possibilities for realizing DUV emitters with emission wavelengths all the way down to 220 nm.

Novel DUV device concept

A novel DUV emitter device concept has been proposed and explored to potentially overcome the intrinsic problem of low p-type conductivity (or low free hole concentration) in Al-rich AlGaN [87]. Figure 10 illustrates our basic novel DUV emitter layer structure based on the band edge alignment between hBN and w-AlN (figure 9(*b*)) and doping engineering. The

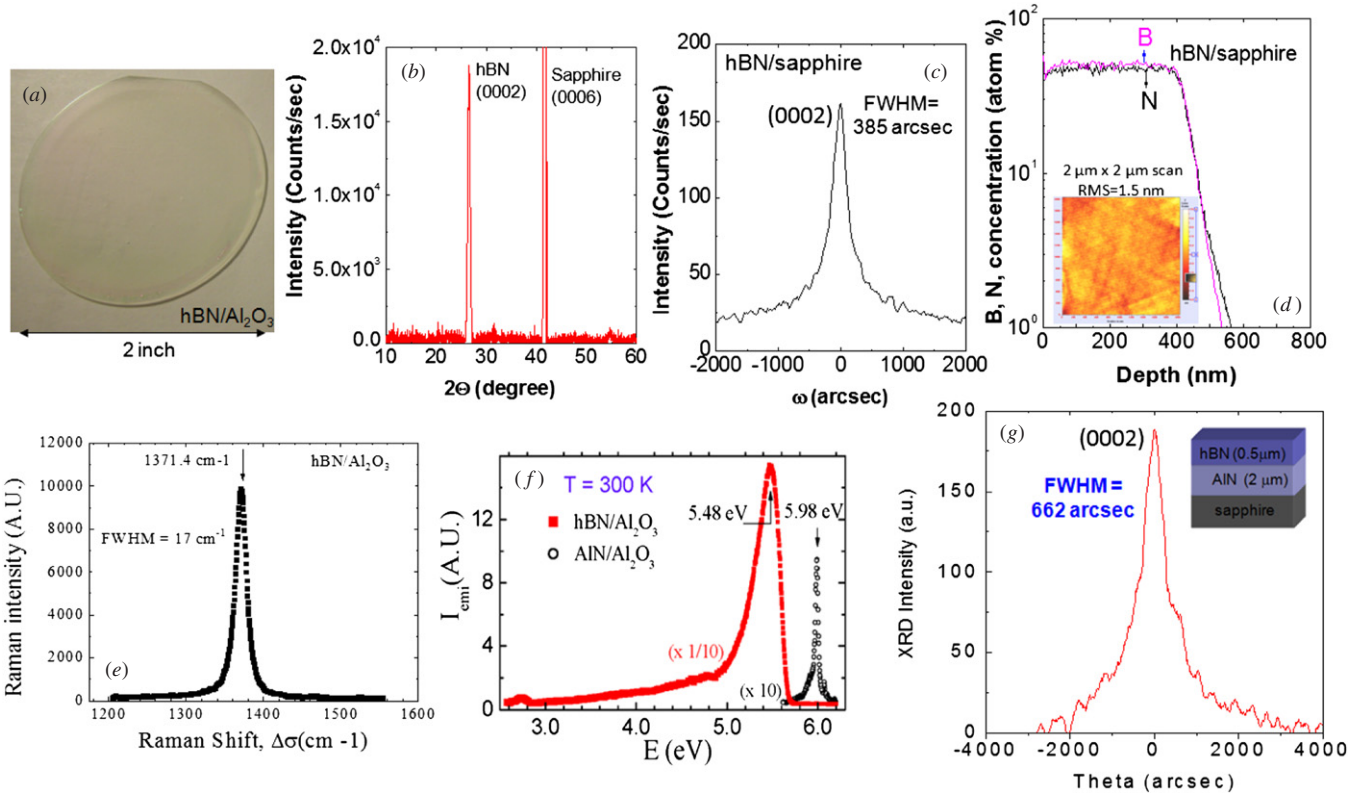

Figure 11. (*a*)–(*e*) Properties of 2 inch hBN epilayers grown on sapphire: (*a*) photo of a 2 inch hBN epilayer wafer, (*b*) XRD θ-2θ scan, (*c*) rocking curve (ω-scan) of the (0 0 0 2) diffraction peak, (*d*) SIMS data obtained for a 0.5 μm thick hBN epilayer and the inset is an AFM image showing the surface morphology with a RMS roughness of about 1.5 nm, (*e*) Raman spectrum, and (*f*) comparison of PL spectra of hBN and AlN [Refs. 86, 88]. (*g*) XRD rocking curve (ω-scan) of the (0 0 0 2) diffraction peak of hBN epilayers deposited on AlN-epilayer/sapphire templates [Ref. 77].

distinctive advantageous features of our novel structure include the following.

(1) Enhanced hole injection efficiency: by implementing the wide bandgap (~6 eV) and highly conductive hBN p-type layer strategy in nitride DUV LEDs, p-type conductivity of the electron blocking layer will be dramatically increased. This will significantly improve the free hole injection and QE, reduce the operating voltage and heat generation, and increase the device operating lifetime

(2) Reduced contact resistance and increased UV transparency: highly conductive hBN will also be used as a p-contact layer. The contact resistance, operating voltage and light absorption in the DUV spectral region will be dramatically reduced compared to the conventional approach of using a p-GaN contact layer. For hBN epilayers, the measured transmission is nearly 100% for photons with $\lambda > 230$ nm.

Current status of hexagonal boron nitride epi-growth

The novel DUV emitter structure is based on our recent efforts on synthesizing wafer-scale hBN epilayers and demonstration of p-type hBN by Mg doping. By leveraging advances in AlN epi-growth, we have recently demonstrated the growth of 2 inch hBN epilayers on sapphire (figure 11(*a*)), AlN/sapphire template, and SiC substrates by MOCVD [77, 80, 84–89]. Figure 11 shows the basic properties of our hBN epilayers. The hBN epilayers were grown using low pressure MOCVD using hydrogen as a carrier gas. The precursors for boron and nitrogen are tri-ethyl boron (TEB) and ammonia (NH_3), respectively. For the growth of hBN epilayers, the typical V/III ratio employed was around 3000. A pulsed growth scheme (alternating flows of TEB and NH_3) was undertaken to minimize the pre-reaction between TEB and ammonia, which is important for obtaining epilayers in hexagonal phase. Due to the lattice mismatch between hBN and Al_2O_3, a low temperature BN buffer layer of about 10 nm in thickness was deposited on the sapphire substrate prior to the growth of hBN epilayer. The growth temperature used to produce hBN epilayers reported in this work was between 1300–1350 °C. The XRD θ-2θ scan of hBN shown in figure 11(*b*) revealed a *c*-lattice constant ~6.67 Å, which closely matches to the bulk *c*-lattice constant of hBN ($c = 6.66$ Å) [90–92], affirming that our MOCVD grown BN films are of single *hexagonal* phase. Figure 11(*c*) is the XRD rocking curve (ω-scan) of the (0 0 0 2) diffraction peak of a 0.5 μm thick hBN film. The observed linewidth (385 arcsec) is comparable to those of typical GaN epilayers grown on sapphire with a similar thickness [93]. Secondary ion mass spectrometry (SIMS) results shown in figure 11(*d*) revealed that hBN epilayers have excellent stoichiometry. As shown in the inset of figure 11(*d*), thin hBN epilayers (<1 μm) exhibit good surface morphologies and RMS values around 1.5 nm can be obtained. However,

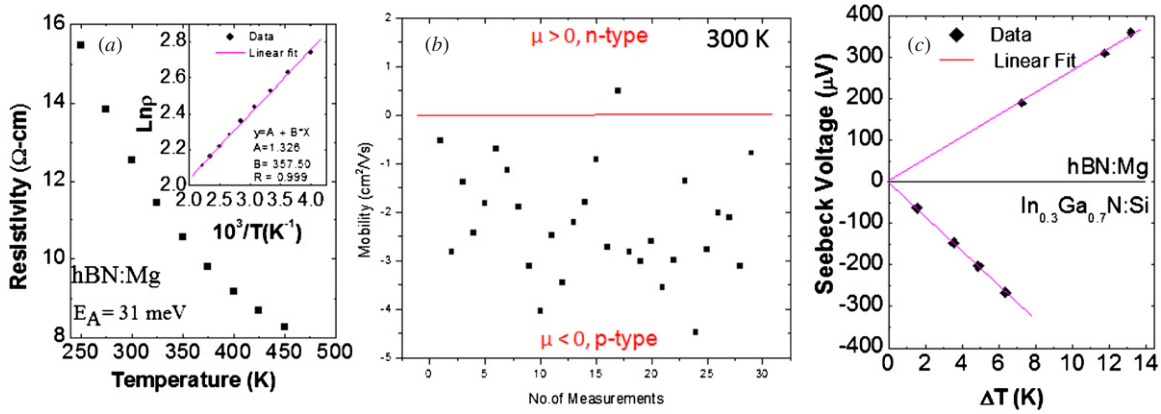

Figure 12. (*a*) p-type resistivity as a function of temperature of an hBN:Mg epilayer in linear scale and the inset shows the same plot in semi-log scale. (*b*) Confirmation of p-type conduction in hBN:Mg at 300 K is obtained by mobility (μ) measurements. In our experimental setup, $\mu > 0$ means electron conduction and $\mu < 0$ means hole conduction. The measured data provide an average hole mobility of $\sim$2 cm^2/V $\cdot$ s. (*c*) The Seebeck coefficients of a hBN:Mg sample and n-type $In_{0.3}Ga_{0.7}N$:Si (with $n = 3 \times 10^{19}$ cm^{-3} and $\mu = 90$ cm^2/V $\cdot$ s) confirm unambiguously that hBN:Mg epilayers are p-type [after Ref. 86].

the surface morphologies of hBN epilayers become poorer with an increase in hBN layer thickness. Figure 11(*e*) is a Raman spectrum of an hBN epilayer. The mode at $\sigma = 1371$ cm^{-1} is attributed to the E_{2g} symmetry vibration in hBN, corresponding to the in-plane stretch of *B* and *N* atoms [94]. Moreover, as shown in figure 11(*f*), the measured band edge PL emission intensity of hBN is two orders of magnitude higher than that of high-quality AlN, attributed primarily to the 2D layered structure of hBN [95]. These results signify that it is feasible to obtain hBN epilayers with high crystalline quality by MOCVD.

In order to realize the novel DUV emitter structure shown in figure 10, the ability of epitaxial growth of hBN on AlGaN is a prerequisite. The feasibility of depositing hBN epilayers on AlN templates has been studied [77]. As shown in figure 11(*g*), the observed linewidth of the (0 0 0 2) XRD rocking curves for hBN epilayers deposited on AlN templates is still broader than those deposited directly on sapphire substrates (with low temperature buffer layers) at this stage.

One of the most significant advantages of hBN over AlN and hBN for DUV device applications is the expected lower acceptor energy level in hBN than in AlN. To demonstrate this, the growth of Mg-doped hBN was conducted by MOCVD and biscyclopentadienyl-magnesium was transported into the reactor during hBN epilayer growth [86]. Mg-doping concentration in the epilayers was about 1×10^{19} cm^{-3}, as verified by SIMS measurement (performed by Charles and Evan). The estimated E_A value in hBN:Mg is around 31 meV based on the temperature-dependent resistivity measurement shown in figure 12(*a*) [86]. The measured E_A value could be lower than the value expected from the effective mass theory due to the effects of relatively heavy doping and layered structure of hBN. The Hall-effect measurement results are shown in figures 12(*a*) and (*b*). Although the mobility data shown in figure 12(*b*) are accompanied by a large fluctuation due to the low hole mobility of our current Mg-doped hBN epilayers, the results confirmed p-type conduction with a free hole concentration P $\sim 10^{18}$ cm^{-3} and an average mobility $\mu \sim 2$ cm^2/V $\cdot$ s. The measured free hole concentration is lower than that estimated from acceptor activation and SIMS data due to the fact that our hBN:Mg epilayers still possess appreciable concentrations of defects which may act as free hole compensating centers. At this point, the origin of the compensating defects is unclear.

Due to the low value of the hole mobilities of the current p-type materials, we also performed Seebeck effect measurements (or the hot probe method) to further confirm the conductivity type of hBN:Mg epilayers [86]. As shown in figure 12(*c*), the Seebeck coefficient for Si-doped $In_{0.3}Ga_{0.7}N$ was $S = \Delta V/\Delta T + S_{\text{Alumel}} = -42.2 - 18.5 = -60.7$ μV K^{-1}, while for hBN:Mg was $S = \Delta V/\Delta T + S_{\text{Alumel}} = 28.0 - 18.5 = 9.5$ μV K^{-1}. The sign reversal in *S* over n-type $In_{0.3}Ga_{0.7}N$:Si sample confirms unambiguously that hBN:Mg epilayers are p-type. The Seebeck effect measurement is a well-established technique to distinguish between n-type and p-type conductivity of a semiconductor [96].

The results shown in figure 12 indicate that this batch of Mg-doped hBN (hBN:Mg) epilayers exhibits a p-type resistivity of around 12 $\Omega \cdot$ cm at 300 K, which is five–six orders of magnitude reduction compared to those of Mg-doped AlN. However, the p-type resistivity of hBN is still five to six times higher than the typical value of about 1 $\Omega \cdot$ cm in Mg-doped GaN (with P $\sim 2 \times 10^{18}$ cm^{-3} and $\mu \sim 10$ cm^2/V $\cdot$ s). Nevertheless, the DUV transparency of the hBN/AlGaN device structure shown in figure 10 is superior to the GaN/AlGaN device structure shown in figure 1.

Demonstration of the hBN/AlGaN p–n junction

In order to realize the novel DUV emitter structure shown in figure 10, the basic growth processes for depositing p-hBN on n-AlGaN must be developed. We have carried out preliminary studies on the growth of p-hBN/n-$Al_xGa_{1-x}N$ ($x \sim 0.62$) heterostructures [77]. The hBN epilayers were grown on AlN and n-$Al_xGa_{1-x}N$ ($x \sim 0.62$) templates. The 1 μm thick Si-doped n-AlGaN epilayer templates were grown by MOCVD on 2 inch (0 0 0 1) sapphire substrates and generally exhibit an n-type conductivity of about 0.01 Ω cm.

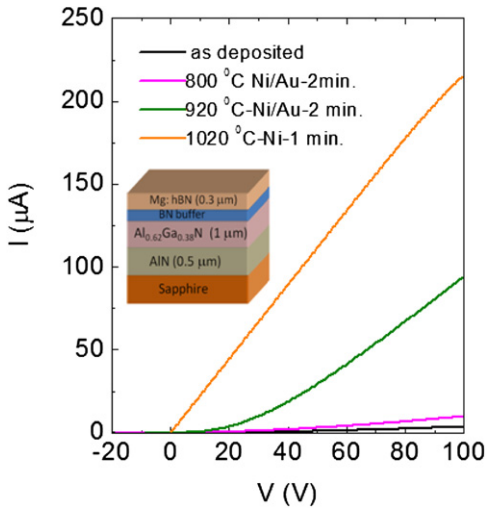

Figure 13. *I–V* characteristics of the Mg-doped p-type hBN epilayers deposited on Si-doped n-AlGaN with Ni/Au and Ni contacts annealed at different times and temperatures [after Ref. 77].

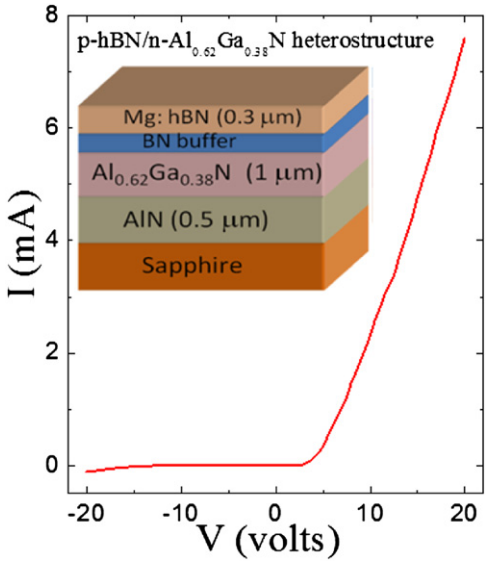

Figure 14. *I–V* characteristics and schematic illustration of a p-BN:Mg/n-$Al_{0.62}Ga_{0.38}N$/AlN p–n structure in which the buffer layer was doped with Mg and p-contacts were annealed at 1020 °C exhibiting a diode behavior [after Ref. 77].

Prior to the n-AlGaN epilayer growth, a 0.5 μm undoped AlN epilayer was first deposited on a sapphire substrate to serve as a template and dislocation filter. For the growth of Mg-doped hBN, biscyclopentadienyl-magnesium was transported into the reactor during hBN epilayer growth. The growth is carried out under nitrogen-rich condition and the variation of NH_3 exposure time did not change the quality of the films, as the growth rate is independent of the NH_3 flow rate. Increase in TEB flow rate increases the growth rate and may also reduce the number of boron vacancies. A low temperature BN buffer layer grown at 800 °C is incorporated before the growth of the hBN epilayer. It has been observed that without this buffer layer, the adhesivity of hBN layers on top of the templates is compromised and the epilayer tends to peel or gets cracked very easily. We have studied the impact of this buffer layer thickness on the quality of the epilayers and have arrived at the optimum buffer layer thickness required to grow better quality hBN epilayers. The thickness of this BN buffer layer was decreased from 140 to 20 nm. An increase in XRD intensity and also a reduction in the full width at half maximum (FWHM) of the hBN epilayers was observed as the buffer layer thickness was decreased.

The XRD θ-2θ scan of hBN/AlN/Al_2O_3 with the hBN (0 0 2) and AlN (0 0 2) peaks placed at 26.5° and 36.0°, respectively. The (0 0 2) peak of the hBN epilayer yields a corresponding lattice constant of $c = 6.70$ Å, which is very close to the hexagonal phase lattice constant of 6.66 Å and the c-lattice constant (6.67 Å) of the hBN epilayers grown on the sapphire substrate shown in figure 11(a). The rocking curve of this (0 0 2) reflection, shown in figure 11(g), has a FWHM of 662 arcsec, which is larger than those grown on sapphire (385 arcsec) indicating that the growth conditions can be further improved.

Similar to the AlGaN materials system [93, 97], the post-growth thermal annealing process is generally necessary to activate Mg acceptors in Mg-doped hBN epilayers. The as-grown samples were annealed at a temperature of 1150 °C for 45 min under a nitrogen ambient atmosphere in order to activate the Mg acceptors. This process renders a p-type resistivity of ∼2.3 Ω cm for Mg-doped hBN epilayers grown on insulating templates [77]. For p-type hBN on n-$Al_{0.62}Ga_{0.38}N$/AlN/Al_2O_3 p-n structure, the sample was etched down to the n-$Al_{0.62}Ga_{0.38}N$ layer using inductively coupled plasma (ICP) dry etching processing [98] and n-contacts consisting of 30 nm thick Ti, 100 nm thick Al, 30 nm thick Ni and 100 nm thick Au metal layers were deposited. The n-contacts were then subjected to thermal treatment (1050 °C for 5 s in nitrogen ambient) in order to decrease the contact resistance and enhance the ohmic behavior of these contacts. P-contacts were formed by depositing 30 nm thick Ni and 120 nm thick Au layers on the top Mg-doped p-type hBN. These processes were adapted and evolved from those of AlGaN [97].

The current–voltage (I–V) characteristics of p-type hBN on the n-$Al_xGa_{1-x}N$/AlN/Al_2O_3 p–n structure were measured at room temperature to investigate the effect of different annealing conditions on the properties of the vertical transport and ohmic contacts to p-hBN grown on n-$Al_{0.62}Ga_{0.38}N$/AlN/Al_2O_3 templates. The I–V characteristics with different annealing conditions are shown in figure 13, which shows that thermal annealing of the contacts is critical and annealing under N_2 ambient above 920 °C for 2 min provides good ohmic contacts. We have noticed that at a temperature greater than 1000 °C the Ni/Au contacts fuse together to form an alloy and tend to get detached from the Mg-doped p-type hBN layer. However, with just the 30 nm Ni layer without Au, annealing at 1020 °C for 2 min makes the contacts ohmic and the contact resistance is drastically reduced. However, the measurements on the ohmic contact resistance and comparison with p-GaN via the transmission line method remain to be conducted.

In addition to the need of thermal annealing treatment of the p-contacts, we also found that doping the buffer

layer with Mg significantly improves the vertical transport properties. Figure 14 shows the *I–V* characteristics and schematic illustration of a p-hBN/n-$Al_xGa_{1-x}N$ ($x \sim 0.62$) structure in which the buffer layer was doped with Mg and p-contacts were annealed at 1020 °C [77]. As can be seen from figure 14, a decent diode behavior in hBN:Mg/n-AlGaN structure has been demonstrated. The leakage current under reverse bias can be controlled to be quite low (~ 3 μA at -10 V). However, DUV emission under current injection has not yet been achieved. We believe that the key parameters to be further optimized are the growth and p-type doping conditions of the low temperature buffer layer.

Summary

Of the many challenges for the development of AlGaN-based DUV photonic devices, n-type conductivity control in Al-rich AlGaN is no longer considered an issue for DUV emitter implementation. By growth optimization to reduce the densities of cation vacancies and their complexes, a room temperature n-type resistivity on the order of $0.01\Omega \cdot$cm can be produced routinely for $Al_xGa_{1-x}N$ ($x \sim 0.7$). The issue of the inherent edge emission property of AlN and Al-rich AlGaN can also be tackled by the formation of deep surface features and carefully designing the active QWs to alter the valence-band order and hence the symmetry of the top valence band in Al-rich AlGaN QWs. The most outstanding technological challenge remaining to be overcome is the low conductivity of p-type AlGaN, which is inherent to AlGaN. This issue is caused by the large acceptor activation energies (E_A) of $Al_xGa_{1-x}N$. A novel DUV emitter device concept based on hBN/AlGaN heterostructure and doping engineering to potentially overcome the intrinsic problem of low p-type conductivity (or low free hole concentration) in Al-rich AlGaN has been proposed and explored. Epitaxial growth of p-type hBN on n-type Al-rich AlGaN has been demonstrated. Diode structures consisting of p-type hBN on n-type Al-rich $Al_xGa_{1-x}N$ have been fabricated and characterized. Thermal annealing of the p-contacts was performed to study the effects of different annealing conditions. The p-hBN/n-AlGaN heterostructures revealed decent diode behaviors with very low reverse leakage currents. Further improvements in material quality, p-type conductivity, the type of ohmic contacts, and post-growth processes would enhance the properties of these p–n structures, which could *ultimately pave the way* toward the realization of high efficiency nitride DUV optoelectronic devices.

Acknowledgments

The effort on hBN/AlGaN heterojunction deep UV device fabrication has been supported by the DARPA-CMUVT program (FA2386-10-1-4165). The studies of the fundamental optical and transport properties of III-nitrides are supported by DOE (DE-FG02-09ER46552) and the studies of the basic structural properties of hBN are supported by NSF (DMR-1206652). The authors are grateful to Dr Jing Li and Dr Su-Huai Wei for insightful discussions and to all the group members in the Center for Nanophotonics at Texas Tech University for their contributions and to the AT&T Foundation for the support of Ed Whitacre and Linda Whitacre endowed chairs.

References

[1] Khan A, Balakrishnan K and Katona T 2008 Ultraviolet light-emitting diodes based on group three nitrides *Nature Photonics* **2** 77
[2] Carrano J and Khan A 2003 Ultraviolet light *SPIE's OE Magazine* p 20
[3] Asif Khan M and Fareed Q 2010 Ultraviolet light emitting devices and methods of fabrication *US Patent Specification* 0032647
[4] Sun W H, Zhang J P, Adivarahan V, Chitnis A, Shatalov M, Wu S, Mandavilli V, Yang J W and Khan M A 2004 AlGaN-based 280 nm light-emitting diodes with continuous wave powers in excess of 1.5 mW *Appl. Phys. Lett.* **85** 531
[5] Mayes K, Yasan A, McClintock R, Shiell D, Darvish S R, Kung P and Razeghi M 2004 High-power 280 nm AlGaN light-emitting diodes based on an asymmetric single-quantum well *Appl. Phys. Lett.* **84** 1046
[6] Fischer A J, Allerman A A, Crawford M H, Bogart K H A, Lee S R, Kaplar R J, Chow W W, Kurtz S R, Fullmer K W and Figiel J J 2004 Room-temperature direct current operation of 290 nm light-emitting diodes with milliwatt power levels *Appl. Phys. Lett.* **84** 3394
[7] Kim K H, Fan Z Y, Khizar M, Nakarmi M L, Lin J Y and Jiang H X 2004 AlGaN-based ultraviolet light-emitting diodes grown on AlN epilayers *Appl. Phys. Lett.* **85** 4777
[8] Nakarmi M L, Kim K H, Khizar M, Fan Z Y, Lin J Y and Jiang H X 2005 Electrical and optical properties of Mg-doped $Al_{0.7}Ga_{0.3}N$ alloys *Appl. Phys. Lett.* **86** 092108
[9] Khizar M, Fan Z Y, Kim K H, Lin J Y and Jiang H X 2005 Nitride deep ultraviolet light-emitting diodes with microlens array *Appl. Phys. Lett.* **86** 173504
[10] Fujioka A, Tasaki T, Murayama T, Narukawa Y and Mukai T 2010 Improvement in output power of 280 nm deep ultraviolet light emitting diode by using AlGaN multi quantum wells *Appl. Phys. Express* **3** 041001
[11] Hirayama H, Tsukada Y, Maeda T and Kamata N 2010 Marked enhancement in the efficiency of deep-ultraviolet AlGaN light-emitting diodes by using a multiquantum-barrier electron blocking layer *Appl. Phys. Express* **3** 031002
[12] Fan Z Y, Lin J Y and Jiang H X 2007 Achieving conductive high Al-content AlGaN alloys for deep UV photonics *Proc. SPIE* **6479** 64791I
[13] Shatalov M *et al* 2010 Large chip high power deep ultraviolet light-emitting diodes *Appl. Phys. Express* **3** 062101
[14] Shatalov M *et al* 2012 AlGaN deep-ultraviolet light-emitting diodes with external quantum efficiency above 10% *Appl. Phys. Express* **5** 082101
[15] Grandusky J R, Chen J, Gibb S R, Mendrick M C, Moe C G, Rodak L, Garrett G A, Wraback M and Schowalter L J 2013 270 nm pseudomorphic ultraviolet light-emitting diodes with over 60 mw continuous wave output power *Appl. Phys. Express* **6** 032101
[16] Pernot C *et al* 2010 Improved efficiency of 255–280 nm AlGaN-based light-emitting diodes *Appl. Phys. Express* **3** 061004
[17] Kinoshita T *et al* 2012 Deep-ultraviolet light-emitting diodes fabricated on AlN substrates prepared by hydride vapor phase epitaxy *Appl. Phys. Express* **5** 122101
[18] Nam K B, Li J, Nakarmi M L, Lin J Y and Jiang H X 2004 Unique optical properties of AlGaN alloys and related ultraviolet emitters *Appl. Phys. Lett.* **84** 5264

[19] Li J, Oder T N, Nakarmi M L, Lin J Y and Jiang H X 2002 Optical and electrical properties of Mg-doped p-type $Al_xGa_{1-x}N$ *Appl. Phys. Lett.* **80** 1210

[20] Nam K B, Nakarmi M L, Li J, Lin J Y and Jiang H X 2003 Mg acceptor level in AlN probed by deep ultraviolet photoluminescence *Appl. Phys. Lett.* **83** 878

[21] Nakarmi M L, Nepal N, Ugolini C, Al Tahtamouni T M, Lin J Y and Jiang H X 2006 Correlation between optical and electrical properties of Mg-doped AlN epilayers *Appl. Phys. Lett.* **89** 152120

[22] Taniyasu Y, Kasu M and Makimoto T 2006 An aluminium nitride light-emitting diode with a wavelength of 210 nanometres *Nature* **441** 325

[23] Nakarmi M L, Nepal N, Lin J Y and Jiang H X 2009 Photoluminescence studies of impurity transitions in Mg-doped AlGaN alloys *Appl. Phys. Lett.* **94** 091903

[24] Stampfl C and Van de Walle C G 2002 Theoretical investigation of native defects, impurities and complexes in AlN *Phys. Rev.* B **65** 155212

[25] Van de Walle C G and Neugebauer J 2004 First-principles calculations for defects and impurities: applications to III-nitrides *J. Appl. Phys.* **95** 3851

[26] Stampfl C and Van de Walle C G 1998 Doping of $Al_xGa_{1-x}N$ *Appl. Phys. Lett.* **72** 459

[27] Simon J, Protasenko V, Lian C, Xing H and Jena D 2010 Polarization-induced hole doping in wide-band-gap uniaxial semiconductor heterostructures *Science* **327** 60

[28] Piprek J and Simon Li Z M 2013 Sensitivity analysis of electron leakage in III-nitride light-emitting diodes *Appl. Phys. Lett.* **102** 131103

[29] Li Y, Chen S, Tian W, Wu Z, Fang Y, Dai J and Chen C 2013 Advantages of AlGaN-based 310-nm UV light-emitting diodes with Al content graded AlGaN electron blocking layers *IEEE Photonics J.* **5** 8200309

[30] Taniyasu Y, Kasu M and Makimoto T 2006 Aluminum nitride deep-ultraviolet light emitting diodes *NTT Tech. Rev.* **4** 54–8 https://www.ntt-review.jp/archive/ntttechnical.php?contents=ntr200612054.pdf

[31] www.rikenresearch.riken.jp/eng/frontline/6923.html

[32] Nakarmi M L, Kim K H, Zhu K, Lin J Y and Jiang H X 2004 Transport properties of conductive N-Type Al-Rich $Al_xGa_{1-x}N$ ($x \geqslant 0.7$) *Appl. Phys. Lett.* **85** 3769

[33] Mattila T and Nieminen R M 1997 Point-defect complexes and broadband luminescence in GaN and AlN *Phys. Rev.* B **55** 9571

[34] Gorczyca I, Christensen N E and Svane A 2002 Influence of hydrostatic pressure on cation vacancies in GaN, AlN, and GaAs *Phys. Rev.* B **66** 075210

[35] Nam K B, Nakarmi M L, Lin J Y and Jiang H X 2005 Deep impurity transitions involving cation vacancies and complexes in AlGaN alloys *Appl. Phys. Lett.* **86** 222108

[36] Nepal N, Nakarmi M L, Lin J Y and Jiang H X 2006 Photoluminescence studies of impurity transitions in AlGaN alloys *Appl. Phys. Lett.* **89** 092107

[37] Fan Z Y, Lin J Y and Jiang H X 2007 Achieving conductive high Al-content AlGaN alloys for deep UV photonics *Proc. SPIE* **6479** 64791I

[38] Sedhain A, Lin J Y and Jiang H X 2011 *AlN - properties and applications Handbook of Luminescent Semiconductor Materials* ed L Bergman and J L McHale (Boca Raton, FL: CRC Press) chapter 3

[39] Pantha B N, Lin J Y and Jiang H X 2012 *High quality Al-rich AlGaN alloys GaN and ZnO-based Materials and Devices* ed S J Pearton (Berlin: Springer) chapter 2

[40] Zhang J P *et al* 2003 High-quality AlGaN layers over pulsed atomic-layer epitaxially grown AlN templates for deep ultraviolet light-emitting diodes *J. Electron. Mater.* **32** 364

[41] Li J, Fan Z Y, Lin J Y and Jiang H X Extreme ultraviolet (EUV) detectors based upon aluminum nitride wide bandgap semiconductors *US Patent Specification* 7498645

[42] Pantha B N, Dahal R, Nakarmi M L, Nepal N, Li J, Lin J Y, Jiang H X, Paduano Q S and Weyburne D 2007 Correlation between optoelectronic and structural properties and epilayer thickness of AlN *Appl. Phys. Lett.* **90** 241101

[43] Uehera K, Aota A, Kemeda S and Tsubouchi K 2005 Low propagation loss of atomically-flat surface AlN with low dislocation density for 5 GHz band SAW devices *IEEE Ultrasonic Symp. 2005* p 455 http://ieeexplore.ieee.org/stamp/stamp.jsp?tp=&arnumber=1602891&userType=inst

[44] Zhu K, Nakarmi M L, Kim K H, Lin J Y and Jiang H X 2004 Silicon doping dependence of highly conductive n-type $Al_{0.7}Ga_{0.3}N$ *Appl. Phys. Lett.* **85** 4669

[45] Suzuki M, Uenoyama T and Yanase A 1995 *Phys. Rev.* B **52** 8132

[46] Wei S-H and Zunger A 1996 *Appl. Phys. Lett.* **69** 2719 and references therein

[47] Persson C, Ferreira da Silva A, Ahuja R and Johansson B 2001 *J. Cryst. Growth* **231** 397

[48] Morkoc H 2008 *Handbook of Nitride Semiconductors and Devices. Vol. 1: Materials Properties, Physics and Growth* (New York: Wiley-VCH)

[49] Chen G D, Smith M, Lin J Y, Jiang H X, Wei S-H, Asif Khan M and Sun C J 1996 Fundamental optical transitions in GaN *Appl. Phys. Lett.* **68** 2784

[50] Li J, Nam K B, Nakarmi M L, Lin J Y, Jiang H X, Carrier P and Wei S-H 2003 Band structure and fundamental optical transitions in wurtzite AlN *Appl. Phys. Lett.* **83** 5163

[51] Jiang H X and Lin J Y 2004 *AlN epitaxial layers for UV photonics Optoelectronic Devices: III-Nitride* ed M Razeghi and M Heini (Amsterdam: Elsevier) chapter 7

[52] Shakya J, Knabe K, Kim K H, Li J, Lin J Y and Jiang H X 2005 Polarization of III-nitride blue and ultraviolet light-emitting diodes *Appl. Phys. Lett.* **86** 091107

[53] Morkoc H, Strite S, Gao G B, Lin M E, Sverdlov B and Burns M 1994 Large-band-gap SiC, III–V nitride, and II–VI ZnSe-based semiconductor device technologies *J. Appl. Phys.* **76** 1363

[54] Oder T N, Shakya J, Lin J Y and Jiang H X 2003 III-nitride photonic crystals *Appl. Phys. Lett.* **83** 1231

[55] Oder T N, Kim K H, Lin J Y and Jiang H X 2004 III-nitride blue and ultraviolet photonic crystal light emitting diodes *Appl. Phys. Lett.* **84** 466

[56] Shakya J, Kim K H, Lin J Y and Jiang H X 2004 Enhanced light extraction in III-nitride ultraviolet photonic crystal light-emitting diodes *Appl. Phys. Lett.* **85** 142

[57] Shakya J, Lin J Y and Jiang H X 2004 Time-resolved electroluminescence studies of III-nitride ultraviolet photonic-crystal light-emitting diodes *Appl. Phys. Lett.* **85** 2104

[58] Jin S X, Li J, Li J Z, Lin J Y and Jiang H X 2000 InGaN/GaN quantum well interconnected microdisk light emitting diodes *Appl. Phys. Lett.* **77** 3236

[59] Jiang H X, Jin S X, Li J and Lin J Y 2000 Micro-size LED and detector arrays for mini-displays, hyperbright light emitting diodes, lighting, and UV detector and imaging sensor applications *US Patent Specification* 6,410,940

[60] Jiang H X and Lin J Y 2003 III-nitride quantum devices—microphotonics *CRC Crit. Rev. Solid State Mater. Sci.* ed P Holloway **28** 131

[61] Jiang H X and Lin J Y 2007 *III-nitride micro-cavity light-emitters Wide Bandgap Light-Emitting Materials and Devices* ed G F Neumark, I Kuskovsky and H X Jiang (New York: Wiley-VCH)

[62] Adivarahan V, Wu S, Sun W H, Mandavilli V, Shatalov M S, Simin G, Yang J W, Maruska H P and Asif Khan M 2004

High-power deep ultraviolet light-emitting diodes based on a micro-pixel design *Appl. Phys. Lett.* **85** 1838
[63] Hwang S, Islam M, Zhang B, Lachab M, Dion J, Heidari A, Nazir H, Adivarahan V and Khan A 2011 A hybrid micro-pixel based deep ultraviolet light-emitting diode lamp *Appl. Phys. Express* **4** 012102
[64] Fan Z Y, Jiang H X and Lin J Y 2008 III-nitride micro-emitter arrays: development and applications *J. Phys. D: Appl. Phys.* **41** 094001
[65] Jiang H X, Jin S X, Li J, Shakya J and Lin J Y 2001 III-nitride blue microdisplays *Appl. Phys. Lett.* **78** 1303
[66] Day J, Li J, Lie D, Bradford C, Lin J Y and Jiang H X 2011 III-Nitride full-scale high-resolution microdisplays *Appl. Phys. Lett.* **99** 031116
[67] Lin J Y, Day J, Li J, Lie D, Bradford C and Jiang H X 2011 High-resolution group III nitride microdisplays SPIE Newsroom, December 14
[68] Jiang H X and Lin J Y 2013 Nitride micro-LEDs and beyond—a decade progress review *Opt. Express* **21** A475
[69] Jiang H X, Lin J Y and Jin S X Light emitting diodes for high AC voltage operating and general lighting *US Patents Specifications* 6,957,899; 7,210,819; 7,213,942
[70] Fan Z Y, Jiang H X and Lin J Y 2005 Heterogeneous integrated high voltage DC/AC light emitter *US Patent Specifications* 7,221,044
[71] Fan Z Y, Li J, Jiang H X and Lin J Y 2008 AC/DC light emitting diodes with integrated protection mechanism *US Patent Specification* 7,714,348
[72] Yamaguchi A A 2010 Theoretical investigation of optical polarization properties in Al-rich AlGaN quantum wells with various substrate orientations *Appl. Phys. Lett.* **96** 151911
[73] Lu H, Yu T, Yuan G, Jia C, Chen G and Zhang G Y 2012 Valence subband coupling effect on polarization of spontaneous emissions from Al-rich AlGaN/AlN quantum wells *Opt. Express* **20** 27384
[74] Al Tahtamouni T M, Lin J Y and Jiang H X 2012 Optical polarization in c-plane Al-rich AlN/AlxGa1-xN single quantum wells *Appl. Phys. Lett.* **101** 042103
[75] Schubert E F and Cho J 2010 UV LEDs: electron-beam excitation *Nature Photonics* **4** 735
[76] Nepal N, Nakarmi M L, Jang H U, Lin J Y and Jiang H X 2006 Growth and photoluminescence studies of Zn-doped AlN epilayers *Appl. Phys. Lett.* **89** 192111
[77] Majety S, Li J, Cao X K, Dahal R, Pantha B N, Lin J Y and Jiang H X 2012 Epitaxial growth and demonstration of hexagonal BN/AlGaN p-n junctions for deep ultraviolet photonics *Appl. Phys. Lett.* **100** 061121
[78] Makimoto T, Kumakura K, Kobayashi Y, Akasaka T and Yamamoto H 2012 A Vertical InGaN/GaN light-emitting diode fabricated on a flexible substrate by a mechanical transfer method using BN *Appl. Phys. Express* **5** 072102
[79] Kobayashi Y, Kumakura K, Akasaka T and Makimoto T 2012 Layered boron nitride as a release layer for mechanical transfer of GaN-based devices *Nature* **484** 223
[80] Majety S, Li J, Zhao W P, Huang B, Wei S H, Lin J Y and Jiang H X 2013 Hexagonal boron nitride and ^{6}H-SiC heterostructures *Appl. Phys. Lett.* **102** 213505
[81] Xu Y N and Ching W T 1991 *Phys. Rev.* B **44** 7787
[82] Geim A K and Novoselov K S 2007 *Nature Mater.* **6** 183
[83] Lu M, Bousetta A, Bensaoula A, Waters K and Schultz J A 1996 Electrical properties of boron nitride thin films grown by neutralized nitrogen ion assisted vapor deposition *Appl. Phys. Lett.* **68** 622
[84] Nose K, Oba H and Yoshida T 2006 Electric conductivity of boron nitride thin films enhanced by *in situ* doping of zinc *Appl. Phys. Lett.* **89** 112124
[85] He B *et al* 2009 p-type conduction in beryllium-implanted hexagonal boron nitride films *Appl. Phys. Lett.* **95** 252106
[86] Dahal R, Li J, Majety S, Pantha B N, Cao X K, Lin J Y and Jiang H X 2011 Epitaxially grown semiconducting hexagonal boron nitride as a deep ultraviolet photonic material *Appl. Phys. Lett.* **98** 211110
[87] Jiang H, Majety S, Dahal R, Li J and Lin J 2012 Structures and devices based on boron nitride and boron nitride-III-nitride heterostructures *US Patent application* 13/482,030
[88] Li J, Majety S, Dahal R, Zhao W P, Lin J Y and Jiang H X 2012 Dielectric strength, optical absorption, and deep ultraviolet detectors of hexagonal boron nitride epilayers *Appl. Phys. Lett.* **101** 171112
[89] Li J, Dahal R, Majety S, Lin J Y and Jiang H X 2011 Hexagonal boron nitride epitaxial layers as neutron detector materials *Nucl. Instrum. Methods Phys. Res.* A **654** 417
[90] Siklitsky V Boron Nitride www.ioffe.rssi.ru/SVA/NSM/Semicond/BN/index.html
[91] Rumyantsev S L, Levinshtein M E, Jackson A D, Mohammmad S N, Harris G L, Spencer M G and Shur M S 2001 *Properties of Advanced Semiconductor Materials GaN, AlN, InN, BN, SiC, SiGe* ed M E Levinshtein, S L Rumyantsev and M S Shur (New York: Wiley) pp 67–92
[92] Lynch R W and Drickamer H G 1966 Effect of high pressure on the lattice parameters of diamond, graphite, and hexagonal boron nitride *J. Chem. Phys.* **44** 181
[93] Nakamura S, Fasol G and Pearton S J 2000 *The Blue Laser Diode: the Complete Story* (Berlin: Springer)
[94] Nemanich R J, Solin S A and Martin R M 1980 Light scattering study of boron nitride microcrystals *Phys. Rev.* B **23** 6348
[95] Huang B, Cao X K, Jiang H X, Lin J Y and Wei S H 2012 Origin of the significantly enhanced optical transitions in layered boron nitride *Phys. Rev.* B **86** 155202
[96] Van Zeghbroeck B Principles of semiconductor devices http://ecee.colorado.edu/~bart/book/book/index.html chapter 2
[97] Pearton S J, Zolper J C, Shul R J and Ren F 1999 *J. Appl. Phys.* **86** 1
[98] Grenadier S, Li J, Lin J Y and Jiang H X 2013 Dry etching techniques for active devices based on hexagonal boron nitride epilayers *J. Vac. Sci. Technol.* A **31** 061517